Neuron, Volume *109*

Supplemental information

Munc13-1 is a Ca^{2+}-phospholipid-dependent vesicle priming hub that shapes synaptic short-term plasticity and enables sustained neurotransmission

Noa Lipstein, Shuwen Chang, Kun-Han Lin, Francisco José López-Murcia, Erwin Neher, Holger Taschenberger, and Nils Brose

Figure S1

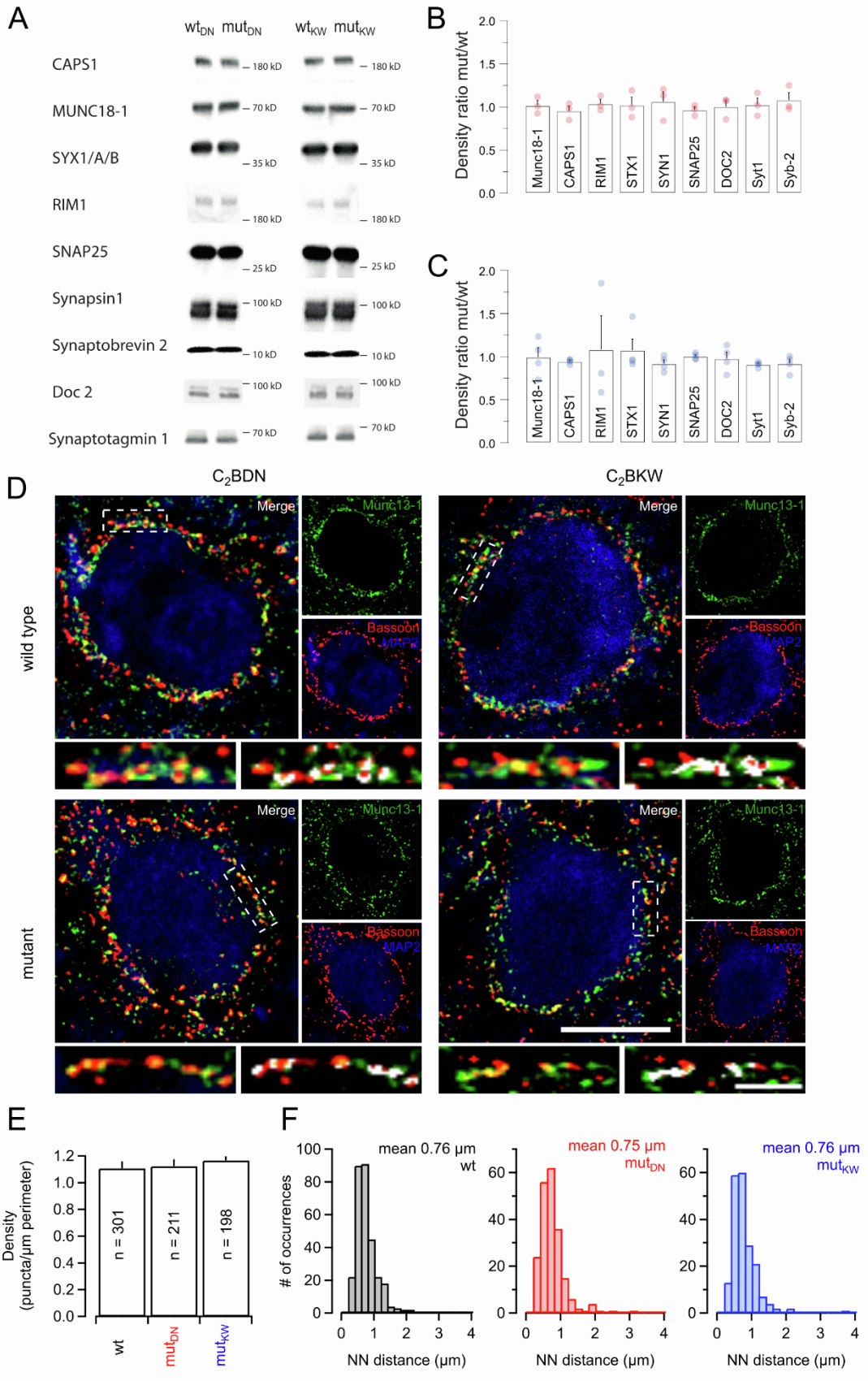
A
wtDN mutDN wtKW mutKW
CAPS1
MUNC18-1
SYX1/A/B
RIM1
SNAP25
Synapsin1
Synaptobrevin 2
Doc 2
Synaptotagmin 1
180 kD
70 kD
35 kD
25 kD
100 kD
10 kD
B
Density ratio mut/wt
Munc18-1
CAPS1
RIM1
STX1
SYN1
SNAP25
DOC2
Syt1
Syb-2
C
D
C2BDN
C2BKW
wild type
mutant
Merge
Munc13-1
Bassoon
MAP2
E
Density (puncta/µm perimeter)
n = 301
n = 211
n = 198
wt
mutDN
mutKW
F
# of occurrences
mean 0.76 µm
wt
mean 0.75 µm
mutDN
mean 0.76 µm
mutKW
NN distance (µm)

Supplemental Figure 1. Quantitative Western Blot Analysis Showing Similar Expression Levels of Munc13-1-Related Proteins in C_2B Mutant Mice and Localization of Munc13-1 in Presynaptic Terminals Surrounding MNTB Principal Neurons (Related to Figure 1)

(A) Example Western blot images of a selection of Munc13-related proteins obtained from P16 cortical lysates.

(B) Quantification for the C_2BDN and (C), C_2BKW mice, showing similar expression levels between C_2B wildtype and mutant mice. Differences in mean density values were statistically not significant ($p>0.05$, ANOVA).

(D) Overlay of Munc13-1 (green), presynaptic AZ marker Bassoon (red), and postsynaptic MAP2 immunofluorescent signals (blue) in confocal images obtained from MNTB sections of P15 wt_{DN} (top left), mut_{DN} (bottom left), wt_{KW} (top right), mut_{KW} (bottom right) mice. Right insets depict Munc13-1 and Bassoon immunofluorescent signals shown in the respective overlays. Bottom insets show the respective regions of interest (ROIs) delineated by the dashed white lines at a higher magnification. Areas of overlap between Munc13-1 and Bassoon immunofluorescent signals are marked in white in the bottom right insets.

(E) Average density of Munc13-1 puncta along the perimeter of the MNTB principal neurons. Data for wt_{DN} and wt_{KW} synapses were similar and therefore pooled. The number of puncta analyzed is given above each bar.

(F) Average distributions of nearest-neighbor distances among Munc13-1 puncta calculated with respect to the center of mass of each punctum for sections obtained from wt (left panel), mut_{DN} (middle panel) and mut_{KW} (right panel) mice.

The analysis shown in (E) and (F) includes all Munc13-1 puncta within a 1 µm wide region of interest drawn around the perimeter of the MNTB principal neuron. The mean puncta density along the PN cell perimeter (~1.1 punctum/µm perimeter; E) and the distribution of nearest-neighbor distances among Munc13-1-positive puncta (F) were indistinguishable between wt and KI samples.

Note that in the images shown in (D) no distinction can be made between Munc13-1 puncta located within processes of calyx terminals and those located in other inhibitory or excitatory small bouton-like synapses.

Scales bars represent 10 µm and 2 µm (inset).

Data in (B), (C) and (E) are represented as mean ± SEM.

Figure S2

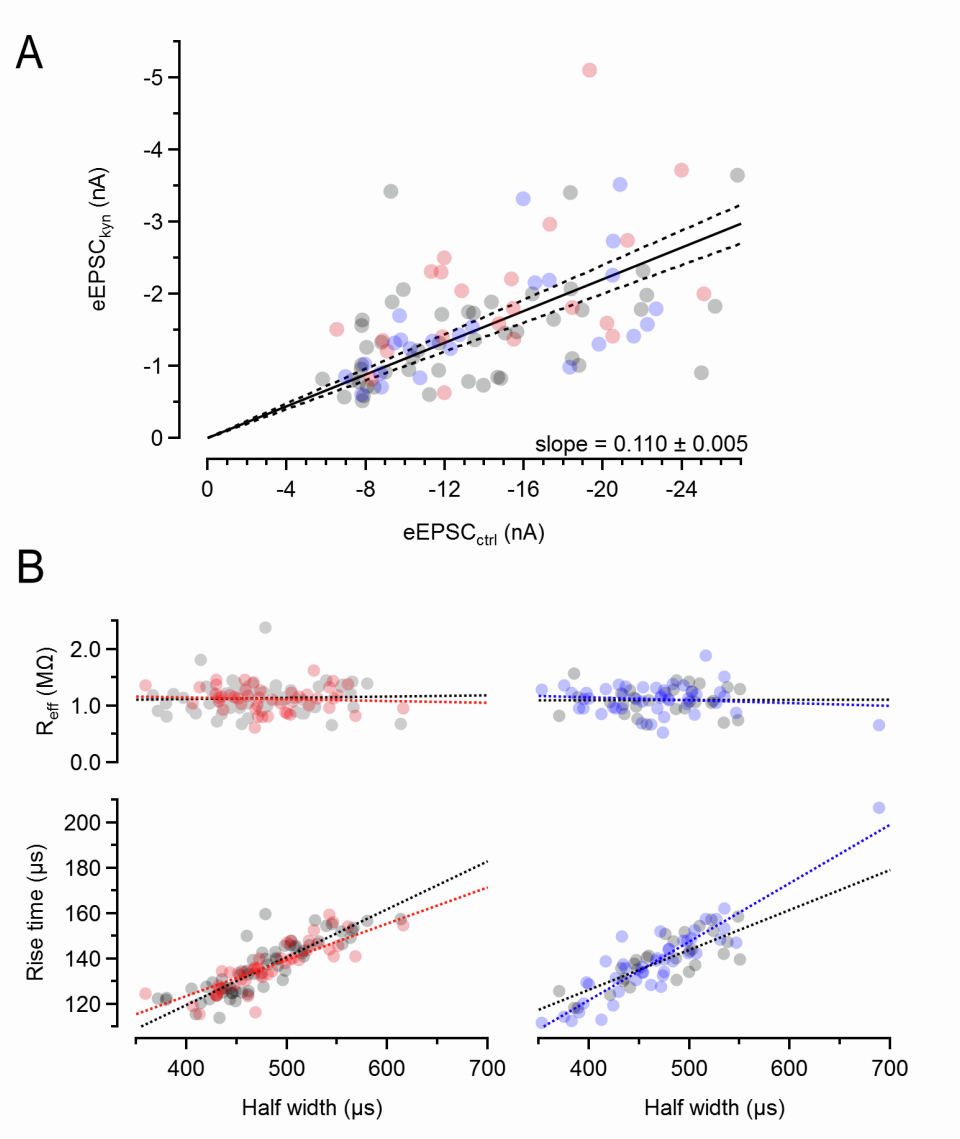
A
eEPSC$_{kyn}$ (nA)
-5
-4
-3
-2
-1
0
slope = 0.110 ± 0.005
0
-4
-8
-12
-16
-20
-24
eEPSC$_{ctrl}$ (nA)
B
R$_{eff}$ (MΩ)
2.0
1.0
0.0
Rise time (µs)
200
180
160
140
120
400
500
600
700
Half width (µs)
400
500
600
700
Half width (µs)

Supplemental Figure 2. Attenuation of Calyceal AMPAR-Mediated eEPSCs by Kynurenic Acid and Positive Correlation of eEPSC Rise-Times and eEPSC Half-Widths (Related to Figure 2)

(A) Unless explicitly indicated otherwise, all eEPSC recordings for this study were obtained in the presence of 1 mM kynurenic acid (kyn) in the bath solution to reduce the size of AMPAR-mediated eEPSCs in order to ensure appropriate voltage-clamp and to minimize postsynaptic AMPAR desensitization and saturation (Neher and Sakaba, 2001; Taschenberger et al., 2002; Wong et al., 2003). In the presence of 1 mM kyn, eEPSC peak amplitudes were reduced to ~11% of control. The figure shows a scatter plot of $eEPSC_{kyn}$ versus $eEPSC_{ctrl}$. Each symbol represents an individual wt (*gray*), mut_{DN} (*red*) or mut_{KW} (*blue*) synapse. Solid and dotted lines represent linear regression (intercept forced to zero) and 95% confidence limits, respectively.

(B) Scatter plots of eEPSC rise times (bottom) and effective series resistance (R_{eff}, top) versus eEPSC half-width. Dotted lines represent linear regressions. Each symbol represents one individual wt (*gray*), mut_{DN} (*red*) or mut_{KW} (*blue*) synapse. R_{eff} is the remaining un-compensated series after routinely applying 82% to 86% electronic access resistance compensation during the recording sessions. R_{eff} was fully compensated during off-line analysis by applying a software correction procedure similarly as described in Traynelis (1998). Note the similar positive correlation between eEPSC rise-times and half-widths most likely reflecting ongoing postnatal developmental acceleration of the eEPSC time course from P14 to P17 as previously reported (Joshi and Wang, 2002; Koike-Tani et al., 2005). The absence of a positive correlation between R_{eff} and eEPSC half-width argues against the possibility that slower eEPSC kinetics is caused by inappropriate voltage-clamp speed. The similar slopes of the regression lines for all genotypes suggest the absence of detrimental effects of the Munc13-1 C_2BDN and C_2BKW mutations on functional synaptic maturation. Data are represented as mean ± SEM.

Figure S3

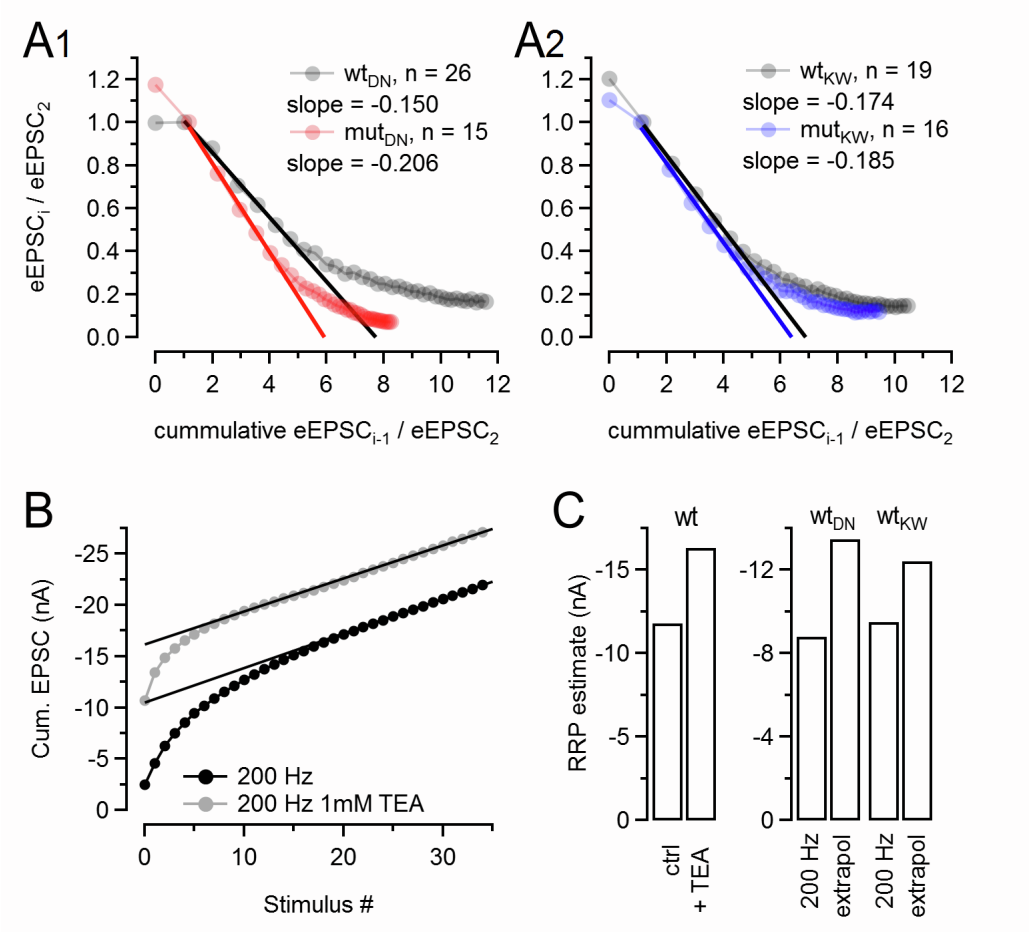
A1
A2
B
C
wtDN, n = 26
slope = -0.150
mutDN, n = 15
slope = -0.206
wtKW, n = 19
slope = -0.174
mutKW, n = 16
slope = -0.185
eEPSCi / eEPSC2
cummulative eEPSCi-1 / eEPSC2
Cum. EPSC (nA)
200 Hz
200 Hz 1mM TEA
Stimulus #
RRP estimate (nA)
wt
wtDN
wtKW
ctrl
+ TEA
200 Hz
extrapol
200 Hz
extrapol

Supplemental Figure 3. Estimating $\bar{p}$ and *FRP* in C_2BDN and C_2BKW Calyx of Held Synapses (Related to Figure 4)

(A) Comparison of estimates for average release probability $\bar{p}$ in C_2BDN (A1) and C_2BKW (A2) calyx synapses. For all stimuli i=1 to 35, eEPSC amplitudes $eEPSC_i$ were plotted against the cumulative previous release $\sum_{n=1}^{i-1} eEPSC_n$ (Elmqvist and Quastel, 1965). The slope of a linear regression within the range $eEPSC_2$ to $eEPSC_6$ represents an estimate for $\bar{p}$. To facilitate comparison among genotypes and also preserve the slopes of the scatter plots, all $eEPSC_i$ and cumulative $eEPSC_i$ were normalized with respect to the peak of $eEPSC_2$. Note the steeper negative slope for mut_{DN} (−0.206) when compared to wt_{DN} synapses (−0.150) indicating higher $\bar{p}$ in the former. For C_2BKW mice, slopes of the regression lines were similar in wt (−0.174) and mut (−0.185) synapses indicating similar $\bar{p}$.

(B) Comparison of pool size estimates obtained from cumulative release measured during 200 Hz eEPSC trains recorded under control conditions (black circles) or in the presence of 1 mM TEA in the bath solution (gray circles). On average, the *FRP* estimate was ~40% larger under conditions when presynaptic Ca^{2+} influx was augmented by extracellular TEA.

(C) The apparent increase in *FRP* size was similar after bath application of TEA (left) compared to that seen when linearly extrapolating the relationship between *FRP* estimate and inter-stimulus interval to ISI = 0 ms (see Figure 4B) (right).

Figure S4

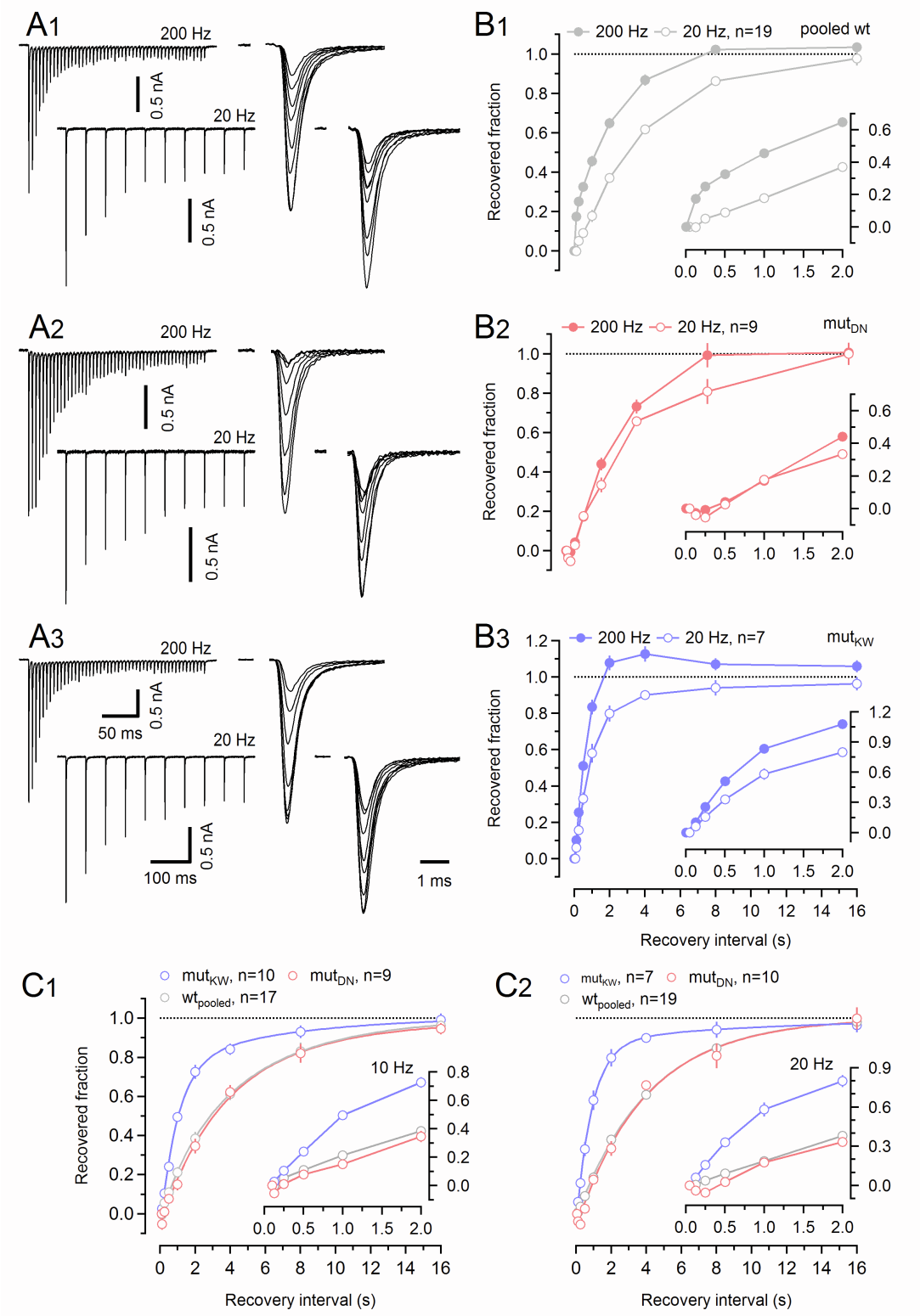
A1
200 Hz
0.5 nA
20 Hz
0.5 nA
A2
200 Hz
0.5 nA
20 Hz
0.5 nA
A3
200 Hz
50 ms
0.5 nA
20 Hz
100 ms
0.5 nA
1 ms
B1
200 Hz
20 Hz, n=19
pooled wt
Recovered fraction
B2
200 Hz
20 Hz, n=9
mutDN
Recovered fraction
B3
200 Hz
20 Hz, n=7
mutKW
Recovered fraction
Recovery interval (s)
C1
mutKW, n=10
mutDN, n=9
wtpooled, n=17
10 Hz
Recovered fraction
Recovery interval (s)
C2
mutKW, n=7
mutDN, n=10
wtpooled, n=19
20 Hz
Recovery interval (s)

Supplemental Figure 4. The Time Course of Recovery of eEPSCs from Synaptic Depression is Slower Following Low-Frequency Conditioning Trains (Related to Figure 5 and 6)

(A, B) Recovery from depression was analyzed in the same synapses after 200 Hz (50 APs, top row) and after 20 Hz (10 APs, bottom row) conditioning trains in wt (A1, B1), mut_{DN} (A2, B2) and mut_{KW} (A3, B3) calyx synapses.

A, Sample traces of conditioning eEPSC trains (left) and $eEPSC_{test}$ recorded after various individual recovery intervals (0.125, 0.25, 0.5, 1, 2, 4, 8 and 16 s).

(B) Average recovery time courses. The recovery time courses shown in (B1) represent pooled data obtained from 12 wt_{DN} and 8 wt_{KW} calyx synapses. In wt synapses (B1), an early rapid component of eEPSC recovery is evident after 200 Hz (filled circles) but absent after 20 Hz (empty circles) conditioning trains. In contrast, mut_{DN} synapses (B2) recover similarly after 20 Hz or 200 Hz conditioning except for the 8 s recovery interval. In mut_{KW} synapses (B3), recovery is generally faster than that in wt_{KW} synapses. In addition, recovery in mut_{KW} synapses occurs substantially faster following 200 Hz conditioning when compared to 20 Hz conditioning trains.

(C) Summary data for experiments such as those illustrated in (A) comparing recovery of eEPSCs from synaptic depression after 10 Hz (C1) and 20 Hz (C2) conditioning trains in Munc13-1 C_2B mut and wt synapses. Data from wt_{DN} and wt_{KW} is pooled in this panel. In C_2BDN mice, mut_{DN} and wt_{DN} synapses showed similar recovery time course after low frequency conditioning trains. In contrast, in C_2BKW mice, mut_{KW} synapses recover substantially faster when compared to wt_{KW} synapses after 10 Hz and 20 Hz conditioning. Insets in (B, C) show the early phase of eEPSC recovery (≤2 s) at an expanded time scale. Data are represented as mean ± SEM.

Figure S5

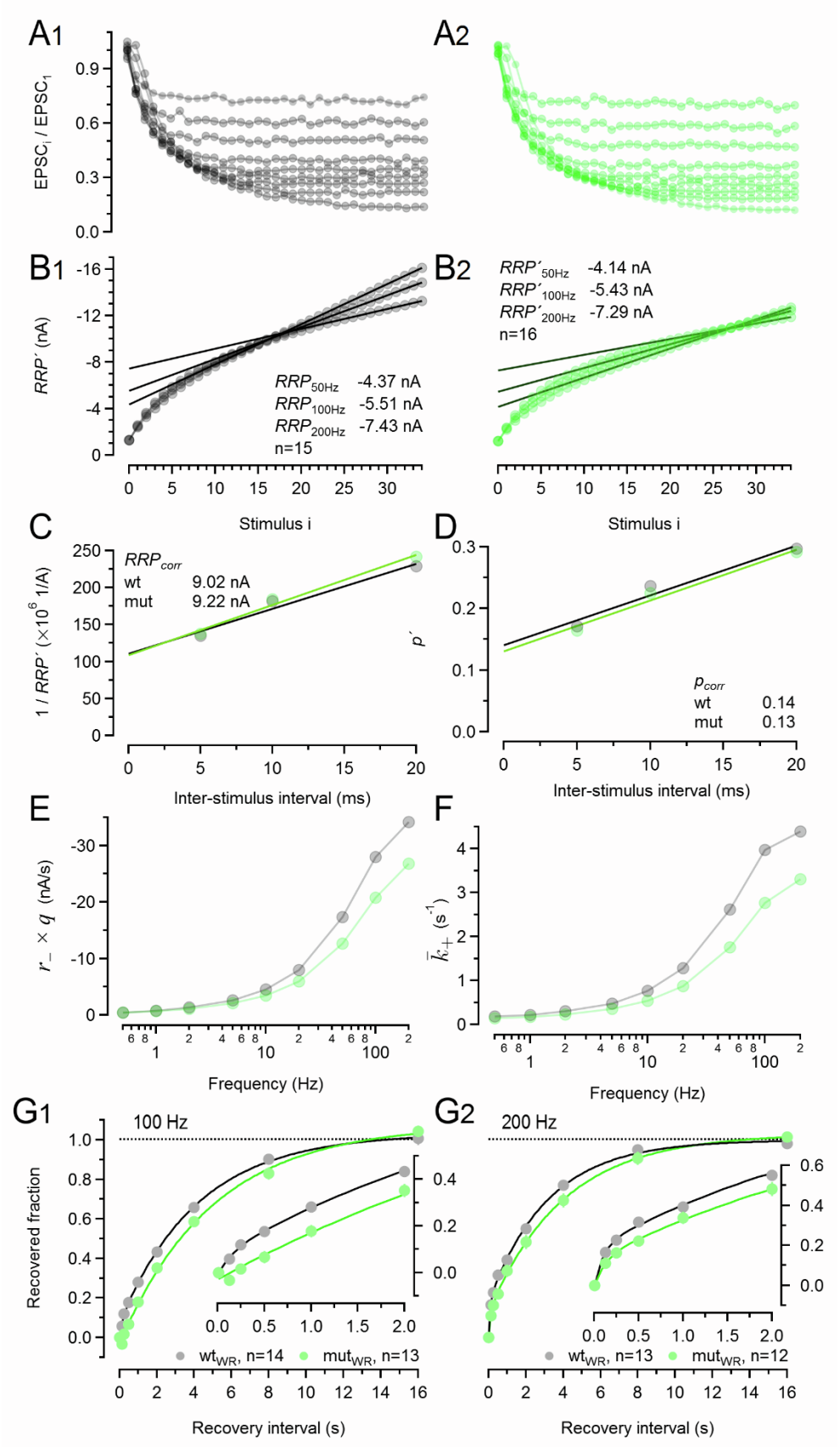
A1
A2
EPSC$_i$ / EPSC$_1$
B1
B2
RRP´ (nA)
RRP$_{50Hz}$ -4.37 nA
RRP$_{100Hz}$ -5.51 nA
RRP$_{200Hz}$ -7.43 nA
n=15
RRP´$_{50Hz}$ -4.14 nA
RRP´$_{100Hz}$ -5.43 nA
RRP´$_{200Hz}$ -7.29 nA
n=16
C
D
Stimulus i
1 / RRP´ (×10^6 1/A)
RRP$_{corr}$
wt 9.02 nA
mut 9.22 nA
p´
p$_{corr}$
wt 0.14
mut 0.13
Inter-stimulus interval (ms)
E
F
r_ × q (nA/s)
$\bar{k}_{+}$ (s^{-1})
Frequency (Hz)
G1
G2
100 Hz
200 Hz
Recovered fraction
wt$_{WR}$, n=14
mut$_{WR}$, n=13
wt$_{WR}$, n=13
mut$_{WR}$, n=12
Recovery interval (s)

Supplemental Figure 5. Short-Term Plasticity Observed during AP Trains in Calyx Synapses of Munc13-1 WR Mice (Related to Figure 5)

Similar experiments as illustrated in Figure 3A,B but recorded in calyx synapses of Munc13-1 WR mice (Lipstein et al., 2013). Note that unlike in Lipstein et a. (2013), all recordings were obtained in the presence of 1 mM kyn.

(A) Average values of normalized eEPSC amplitudes during train stimulation using various frequencies (0.5, 1, 2, 5, 10, 20, 50, 100 and 200 Hz) recorded in wt_{WR} (A1) and mut_{WR} (A2) calyx synapses.

(B) Average values of cumulative eEPSC amplitudes measured during 50, 100 and 200 Hz stimulation in wt_{WR} (B1) and mut_{WR} (B2) calyx synapses. Solid lines represent corrections for ongoing SV pool refilling assuming a constant average replenishment $\bar{r}_+ \times q$. Intersections of these lines with the abscissa represent apparent *FRP* estimates (FRP') for f_{stim} 50, 100 and 200 Hz denoted here as FRP'_{50Hz}, FRP'_{100Hz} *and* FRP'_{200Hz}. Note the increase in FRP' with higher f_{stim}.

(C, D) $1/FRP'$ (C) and apparent average release probability for $eEPSC_1$ ($\bar{p}' = eEPSC_1 / FRP'$, D) plotted as a function of inter-stimulus interval of the stimulus trains. Gray and green symbols represent mean values for wt and mut synapses, respectively. Solid traces represent linear regressions to the scatter plots. Intersections of the line fits with the abscissa (at *ISI* = 0 ms) represent corrected estimates for $1/FRP_{corr}$ (C) and $\bar{p}_{corr}$ (D). Note the similarity of FRP_{corr} and $\bar{p}_{corr}$ estimates for wt_{WR} and mut_{WR} mice.

(E, F) Average steady-state release rates measured in nA/s ($\bar{r}_- \times q$) (E) and average steady state replenishment rate constants $\bar{k}_+$ (F) plotted as a function of f_{stim}. In both wt_{WR} and mut_{WR} calyx synapses, $\bar{r}_- \times q$ and $\bar{k}_+$ increase with higher f_{stim}, albeit to a lesser extent in the mut_{WR}.

(G) Average time course of eEPSC recovery from synaptic depression after 100 Hz (G1) or 200 Hz (G2) conditioning eEPSC trains. Data are represented as mean ± SEM.

Figure S6

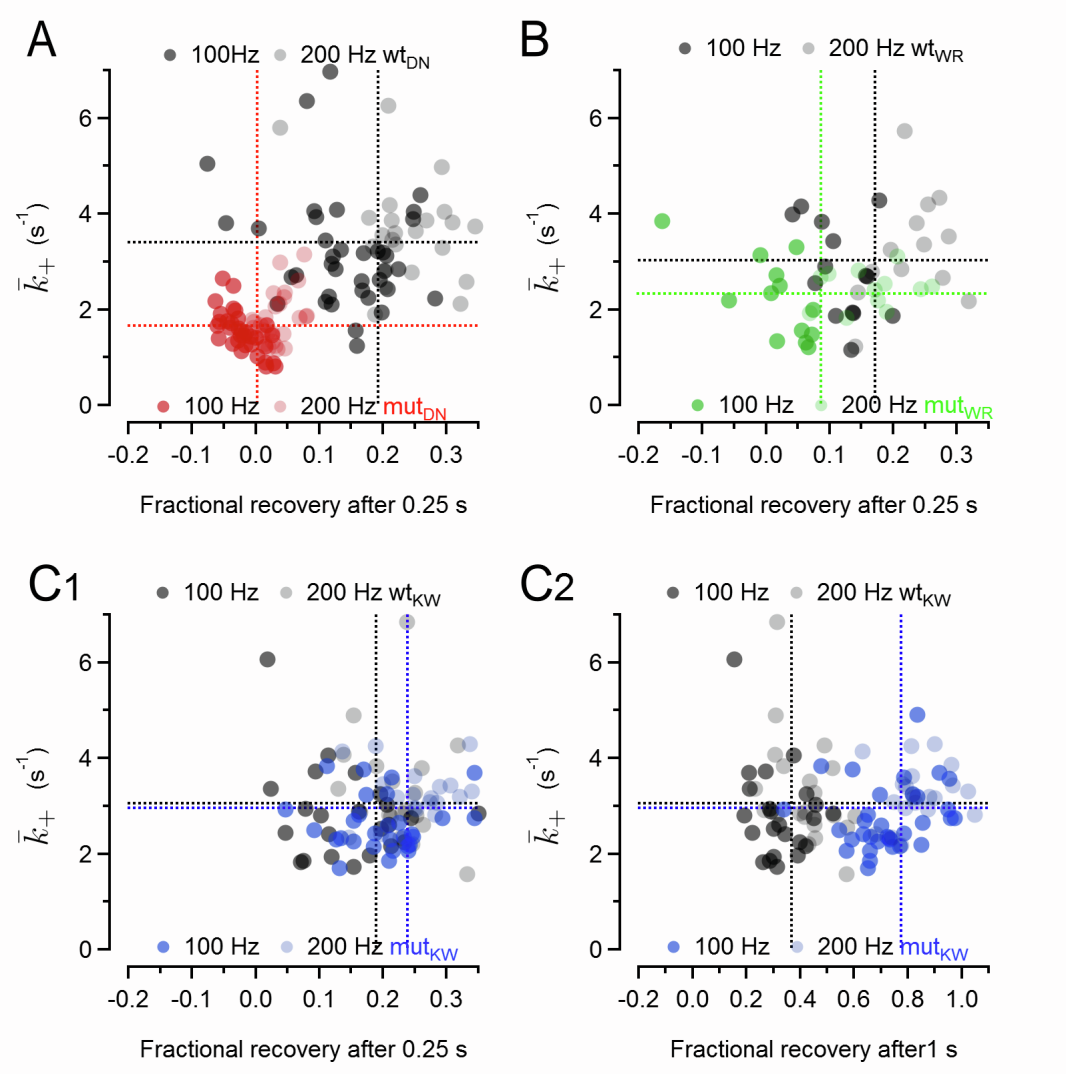
A
100Hz
200 Hz wt$_{DN}$
100 Hz
200 Hz mut$_{DN}$
$\bar{k}_+$ (s^{-1})
Fractional recovery after 0.25 s
B
100 Hz
200 Hz wt$_{WR}$
100 Hz
200 Hz mut$_{WR}$
$\bar{k}_+$ (s^{-1})
Fractional recovery after 0.25 s
C1
100 Hz
200 Hz wt$_{KW}$
100 Hz
200 Hz mut$_{KW}$
$\bar{k}_+$ (s^{-1})
Fractional recovery after 0.25 s
C2
100 Hz
200 Hz wt$_{KW}$
100 Hz
200 Hz mut$_{KW}$
$\bar{k}_+$ (s^{-1})
Fractional recovery after1 s

Supplemental Figure 6. Scatter Plot of Estimated Steady State SV Recruitment Rate Constants During Conditioning Trains versus Fractional Recovery following Conditioning Trains (Related to Figures 4, 5 and 6)

Scatter graphs plotting the apparent replenishment rate constants estimates $\bar{k}_+$ as a function of the fractional eEPSC recovery measured at a recovery interval of 250 ms for individual C_2BDN (A), WR (B) and C_2BKW (C) synapses that were conditioned using 100 Hz (dark symbols) and 200 Hz (light symbols) trains. Each symbol represents a single synapse. Broken lines represent average values obtained from pooled 100 Hz and 200 Hz data.

(A) Among C_2BDN calyx synapses, mut_{DN} synapses showed lower replenishment rate constants during high frequency conditioning (compare to Figure 4E1) and also less recovery 250 ms after cessation of stimulation when compared to wt_{DN} synapses. There was little overlap among data obtained from wt_{DN} and mut_{DN} synapses. Higher $\bar{k}_+$ estimates correlated well with increased fractional recovery measured after 250 ms.

(B) Data obtained from WR mice is similar to that obtained from C2BDN, albeit with less pronounce differences between wt and mut synapses, consistent with the smaller differences between average magnitudes of STD as well as average time courses of recovery from STD observed between wt_{WR} and mut_{WR}.

(C) Calyx synapses of C_2BKW mice show similar steady state replenishment rate constants during 100 Hz and 200 Hz conditioning trains for wt_{KW} and mut_{KW} synapses (compare to Figure 4E2). However, fractional recovery achieved after 250 ms or 1 s recovery interval is slightly (C1) or substantially higher (C2), respectively, in mut_{KW} when compared to wt_{KW} synapses. This indicates that in mut_{KW}, the replenishment of the *FRP* following depletion proceeds considerably faster during the decay of $[Ca^{2+}]_i$ to resting values although SV recruitment rates at the end of the high-frequency conditioning were accelerated to a similar extent in wt and mut C_2BKW synapses.

Figure S7

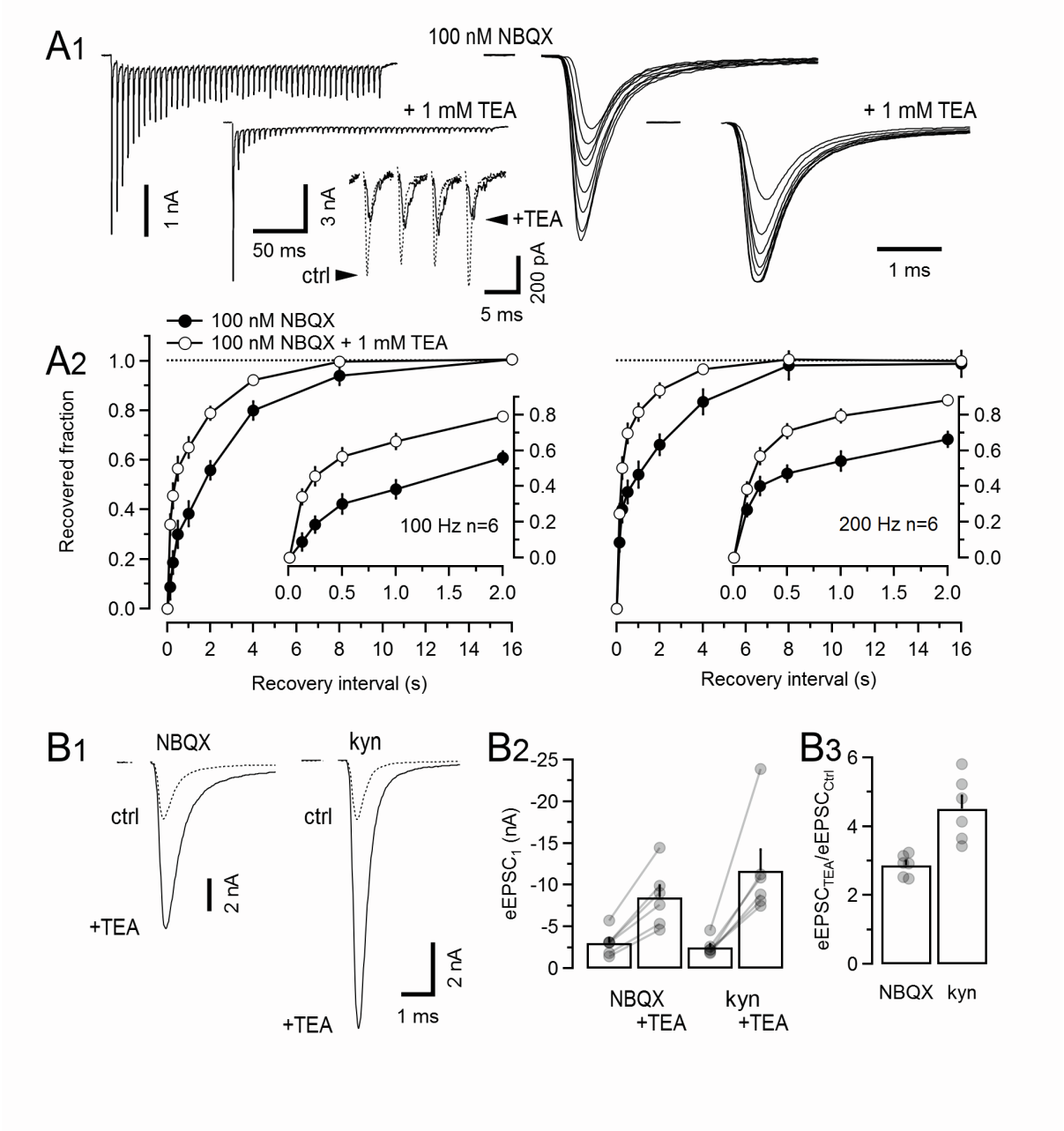
A1
100 nM NBQX
+ 1 mM TEA
1 nA
3 nA
50 ms
+TEA
ctrl
200 pA
5 ms
+ 1 mM TEA
1 ms
A2
100 nM NBQX
100 nM NBQX + 1 mM TEA
Recovered fraction
100 Hz n=6
200 Hz n=6
Recovery interval (s)
B1
NBQX
kyn
ctrl
+TEA
2 nA
1 ms
B2
eEPSC1 (nA)
NBQX +TEA
kyn +TEA
B3
eEPSCTEA/eEPSCCtrl
NBQX
kyn

Supplemental Figure 7. Apparent Speed-Up of SV Replenishment after Augmenting Presynaptic Ca^{2+} Influx under Conditions that Leave AMPAR Desensitization and Saturation Unaffected (Related to Figure 6)

(A) Probing of recovery of eEPSC from depression elicited by conditioning 100 Hz and 200 Hz trains in the absence of kynurenic acid. The bath solution was supplemented with 100 nM NBQX to partially block AMPARs and achieve eEPSC peak amplitudes that were on average similar to those recorded in the presence of 1 mM kyn (compare to Figures 5A, 6A). A1, Sample traces of conditioning eEPSC (left) and $eEPSC_{test}$ recorded after various recovery intervals (right, $eEPSC_{test}$ recorded at 0.125, 0.25, 0.5, 1 ,2, 4, 8 and 16 s recovery shown superimposed) either in the presence of 100 nM NBQX (top row) or in the presence of 100 nM NBQX + 1 mM TEA (bottom row). The inset in the right column compares the last three eEPSC of the conditioning train before (dotted trace) and after (solid trace) application of 1 mM TEA. Note that despite the faster eEPSC recovery time course observed in the presence of TEA, the steady state eEPSC amplitude during conditioning is actually reduced. A2, Average time course of eEPSC recovery from synaptic depression after 100 Hz (left) or 200 Hz (right) conditioning eEPSC trains recorded in the absence (filled circles) or presence (empty circles) of 1 mM TEA. Note the apparent acceleration of recovery in the presence of bath-applied TEA. Insets show the early recovery at an expanded time scale.

(B) Comparison of TEA-induced augmentation of $eEPSC_1$ for recordings with either 100 nM NBQX or 1 mM kyn present in the bath solution. B1, $eEPSC_1$ from panels A1 (left) and from Figure 6D1 (right) are shown superimposed for comparison. B2, Bar graph and scatter dot plot representing average amplitudes and individual measurements, respectively, of $eEPSC_1$ under the different recording conditions. B3, Bar graph and scatter dot plot representing average ratios and individual measurements, respectively, of $eEPSC_1$ augmentation recorded with either 100 nM NBQX (left) or 1 mM kyn (right) present in the bath. Note the substantially larger increase in $eEPSC_1$ amplitudes after application of 1 mM TEA in the presence of 1 mM kyn (right).

The most parsimonious explanation for differences in eEPSC recovery in the absence or presence of a low-affinity, fast off-rate GluR antagonist is that $eEPSC_{ss}$ is affected by receptor desensitization while the initial eEPSC ($eEPSC_1$) and late $eEPSC_{test}$ are affected by receptor saturation. These two postsynaptic mechanisms modulate the eEPSC recovery time course in addition to *FRP* depletion in the following way: (*i*) The initial rapid recovery of $eEPSC_{test}$ immediately after the end of the conditioning train likely reflects – at least in part – fast relief from AMPAR desensitization, and (*ii*) an apparent speed-up of late $eEPSC_{test}$ recovery results

from AMPAR saturation because the amplitude of $eEPSC_{test}$ returns to a maximum that is capped by receptor saturation. This is essentially analogous to the accelerating effect of postsynaptic saturation and desensitization on the recovery from depression induced by single conditioning eEPSCs, which was previously reported for climbing fiber to Purkinje cell synapses (Foster et al., 2002) and auditory brainstem endbulb synapses (Chanda and Xu-Friedman, 2010).

Data are represented as mean ± SEM.

Table S1. Functional parameters of synaptic transmission (related to Figures 2-6).

	wt_{DN}	**mut_{DN}**	statistical significance[1]	**wt_{KW}**	**mut_{KW}**	statistical significance[1]
presynaptic $I_{Ca(V)}$	N=4/n=15	N=5/n=17		N=4/n=13	N=5/n=15	
peak amplitude during 10 ms step to 0 mV (nA)	−1.371 ± 0.102	−1.454 ± 0.096	n.s.	−1.407 ± 0.112	−1.395 ± 0.116	n.s.
charge during 1 ms step to 0 mV (pC)	−0.887 ± 0.088	−0.963 ± 0.063	n.s.	−0.935 ± 0.096	−0.951 ± 0.081	n.s.
$Q_{Ca(V),35}$ / $Q_{Ca(V),1}$	N=5/n=15	N=5/n=17		N=8/n=15	N=7/n=15	
f_{stim} = 5 Hz	1.012 ± 0.006	1.015 ± 0.006	n.s.	1.016 ± 0.005	1.002 ± 0.009	n.s.
f_{stim} = 10 Hz	1.027 ± 0.006	1.034 ± 0.008	n.s.	1.034 ± 0.008	1.026 ± 0.008	n.s.
f_{stim} = 100 Hz	1.309 ± 0.021	1.276 ± 0.024	n.s.	1.294 ± 0.020	1.320 ± 0.020	n.s.
f_{stim} = 200 Hz	1.277 ± 0.021	1.266 ± 0.031	n.s.	1.285 ± 0.023	1.290 ± 0.023	n.s.
single eEPSCs	N=36/n=66	N=23/n=47		N=17/n=29	N=18/n=44	
amplitude (nA) (in 1 mM kyn)	−1.84 ± 0.16	−2.90 ± 0.27	p = 0.001	−1.83 ± 0.28	−1.90 ± 0.16	n.s.
projected amplitude (nA) (w/o kyn) [2]	−16.73 ± 1.45	−26.36 ± 2.45		−16.64 ± 2.54	−17.27 ± 1.45	
half-width (ms)	4.73 ± 0.07	4.8 ± 0.07	n.s.	4.73 ± 0.09	4.63 ± 0.09	n.s.
20-80% rise time	1.34 ± 0.02	1.36 ± 0.02	n.s.	1.36 ± 0.02	1.36 ± 0.02	n.s.
R_{eff} (MΩ)	1.14 ± 0.03	1.12 ± 0.03	n.s.	1.10 ± 0.04	1.11 ± 0.04	n.s.
$eEPSC_2/eEPSC_1$ for two consecutive eEPSCs	N=12/n=26	N=9/n=15		N=11/n=19	N=8/n=16	
ISI = 2000 ms	0.84 ± 0.03	0.82 ± 0.03		0.80 ± 0.03	0.84 ± 0.02	
ISI = 1000 ms	0.83 ± 0.03	0.75 ± 0.02		0.77 ± 0.02	0.82 ± 0.01	
ISI = 500 ms	0.79 ± 0.02	0.73 ± 0.02		0.75 ± 0.02	0.78 ± 0.03	
ISI = 250 ms	0.77 ± 0.02	0.71 ± 0.03		0.71 ± 0.03	0.73 ± 0.02	
ISI = 100 ms	0.77 ± 0.02	0.68 ± 0.02		0.72 ± 0.03	0.73 ± 0.02	
ISI = 50 ms	0.76 ± 0.02	0.68 ± 0.03		0.70 ± 0.04	0.72 ± 0.03	
ISI = 25 ms	0.82 ± 0.02	0.72 ± 0.04		0.76 ± 0.04	0.79 ± 0.04	
ISI = 10 ms	0.9 ± 0.03	0.77 ± 0.04		0.87 ± 0.05	0.83 ± 0.04	
ISI = 5 ms	1.02 ± 0.04	0.91 ± 0.04		0.92 ± 0.05	0.93 ± 0.04	
$eEPSC_{ss}/eEPSC_1$ during eEPSC trains	N=12/n=26	N=9/n=15		N=11/n=19	N=8/n=16	
f_{stim} = 0.5 Hz	0.721 ± 0.018	0.684 ± 0.022	n.s.	0.683 ± 0.017	0.800 ± 0.017	p < 0.001
f_{stim} = 1 Hz	0.619 ± 0.018	0.543 ± 0.024	p = 0.020	0.571 ± 0.020	0.715 ± 0.014	p < 0.001
f_{stim} = 2 Hz	0.521 ± 0.018	0.406 ± 0.024	p < 0.001	0.473 ± 0.021	0.625 ± 0.020	p < 0.001
f_{stim} = 5 Hz	0.430 ± 0.019	0.276 ± 0.022	p < 0.001	0.374 ± 0.020	0.514 ± 0.019	p < 0.001
f_{stim} = 10 Hz	0.376 ± 0.020	0.198 ± 0.020	p < 0.001	0.326 ± 0.020	0.423 ± 0.017	p < 0.001
f_{stim} = 20 Hz	0.337 ± 0.022	0.149 ± 0.016	p < 0.001	0.294 ± 0.020	0.342 ± 0.020	n.s.
f_{stim} = 50 Hz	0.309 ± 0.024	0.115 ± 0.012	p < 0.001	0.255 ± 0.021	0.239 ± 0.015	n.s.
f_{stim} = 100 Hz	0.253 ± 0.022	0.097 ± 0.012	p < 0.001	0.212 ± 0.023	0.174 ± 0.014	n.s.
f_{stim} = 200 Hz	0.171 ± 0.014	0.071 ± 0.008	p < 0.001	0.149 ± 0.019	0.120 ± 0.013	n.s.
***FRP* estimate (nA) [3] (from eEPSC trains)**	−11.60 ± 1.59	−15.44 ± 1.63	n.s.	−10.09 ± 1.66	−12.64 ± 1.72	n.s.
95% conf intervals (nA)	−9.26 … −15.47	−12.45 … −18.80		−7.46 … −13.89	−9.61 … −16.31	
***p* estimate [3] (from eEPSC trains)**	0.112 ± 0.013	0.180 ± 0.015	p < 0.001	0.159 ± 0.025	0.145 ± 0.018	n.s.
95% conf intervals	0.087 … 0.136	0.152 … 0.212		0.115 … 0.212	0.110 … 0.179	

***RRP* estimate by ΔC_m (fF)**	303 ± 25 N=4/n=14	311 ± 16 N=5/n=16	n.s.	351 ± 32 N=4/n=13	349 ± 39 N=4/n=13	n.s.
fractional eEPSC recovery from depression (100 Hz)	N=19/n=37	N=19/n=33		N=15/n=23	N=13/n=33	
interval = 0.125 s	0.072 ± 0.012	−0.031 ± 0.005	$p < 0.001$	0.090 ± 0.014	0.083 ± 0.010	n.s.
interval = 0.25 s	0.139 ± 0.013	−0.019 ± 0.005	$p < 0.001$	0.146 ± 0.017	0.219 ± 0.015	$p = 0.002$
interval = 0.5 s	0.221 ± 0.011	0.026 ± 0.006	$p < 0.001$	0.226 ± 0.021	0.439 ± 0.022	$p < 0.001$
interval = 1 s	0.308 ± 0.016	0.124 ± 0.009	$p < 0.001$	0.322 ± 0.020	0.726 ± 0.025	$p < 0.001$
interval = 2 s	0.481 ± 0.017	0.332 ± 0.012	$p < 0.001$	0.459 ± 0.026	0.947 ± 0.029	$p < 0.001$
interval = 4 s	0.728 ± 0.016	0.621 ± 0.015	$p < 0.001$	0.704 ± 0.022	1.006 ± 0.024	$p < 0.001$
interval = 8 s	0.912 ± 0.013	0.891 ± 0.010	n.s.	0.903 ± 0.022	1.022 ± 0.019	$p < 0.001$
interval = 16 s	0.998 ± 0.016	1.008 ± 0.012	n.s.	0.982 ± 0.015	1.004 ± 0.013	n.s.
fractional eEPSC recovery from depression (200 Hz)	N=16/n=27	N=17/n=27		N=15/n=21	N=12/n=22	
interval = 0.125 s	0.193 ± 0.015	0.013 ± 0.005	$p < 0.001$	0.143 ± 0.015	0.124 ± 0.008	n.s.
interval = 0.25 s	0.266 ± 0.020	0.033 ± 0.005	$p < 0.001$	0.238 ± 0.015	0.269 ± 0.015	n.s.
interval = 0.5 s	0.359 ± 0.020	0.075 ± 0.004	$p < 0.001$	0.320 ± 0.019	0.524 ± 0.020	$p < 0.001$
interval = 1 s	0.458 ± 0.020	0.188 ± 0.009	$p < 0.001$	0.420 ± 0.023	0.851 ± 0.026	$p < 0.001$
interval = 2 s	0.604 ± 0.020	0.408 ± 0.014	$p < 0.001$	0.591 ± 0.024	1.059 ± 0.025	$p < 0.001$
interval = 4 s	0.859 ± 0.020	0.705 ± 0.018	$p < 0.001$	0.811 ± 0.021	1.106 ± 0.020	$p < 0.001$
interval = 8 s	1.018 ± 0.016	0.938 ± 0.012	$p < 0.001$	0.988 ± 0.015	1.077 ± 0.014	$p < 0.001$
interval = 16 s	1.022 ± 0.016	1.017 ± 0.014	n.s.	1.023 ± 0.014	1.035 ± 0.017	n.s.
time constant of eEPSC recovery from depression						
weighted τ (s) (following 100 Hz 25 APs)	3.148	4.204		3.327	0.800	
weighted τ (s) (following 200 Hz 50 APs)	2.145	3.541		2.385	0.663	
weighted τ (s) (following 10 Hz 10 APs)	4.415 [4]	4.775		4.415 [4]	2.387	
weighted τ (s) (following 20 Hz 10 APs)	4.193 [4]	4.210		4.193 [4]	2.015	
decay of global presynaptic $[Ca^{2+}]_i$ following 100 Hz conditioning	N=2/n=6	N=2/n=6		N=2/n=6	N=2/n=5	
decay τ_{fast} (ms)	36.08 ± 0.88	36.65 ± 1.12		38.52 ± 0.69	37.86 ± 0.95	
decay τ_{slow} (ms)	419.9 ± 12.2	458.8 ± 16.3		436.2 ± 8.9	414.1 ± 14.9	
fraction of slow component	0.221	0.221		0.232	0.194	
decay of global presynaptic $[Ca^{2+}]_i$ following 200 Hz conditioning	N=2/n=6	N=2/n=6		N=2/n=6	N=2/n=5	
decay τ_{fast} (ms)	44.05 ± 0.50	44.57 ± 0.60		49.54 ± 0.53	45.47 ± 0.60	
decay τ_{slow} (ms)	393.5 ± 7.6	415.5 ± 10.5		395.1 ± 7.8	359.5 ± 9.84	
fraction of slow component	0.182	0.164		0.175	0.160	

[1] If not stated otherwise, a two-tailed Welch–Satterthwaite t-test was used to test for statistical significance of the differences between sample means.

[2] $EPSC_{kyn}$ × a, where $EPSC_{kyn}$ is the amplitude measured in the presence of 1 mM kynurenic acid and a is the inverse of the average blocking ratio of 1 mM kyn (a = 1/0.11), which was determined in a subset of recordings.

[3] SEM and 95% confidence interval estimates were obtained by bootstrap resampling analysis using a balanced bootstrap approach (every experimental observation appeared exactly the same number of times in the total population of 10,000 bootstrap samples) (Davison et al., 1986; Gleason, 1988).

[4] Results for wt_{DN} and wt_{KW} synapses were similar. Therefore, both, wt_{DN} and wt_{KW}, data sets were pooled to a single wt data set to which the results given here apply.

Supplemental Table 1. Functional parameters of synaptic transmission in P14–18 C_2BDN and C_2BKW mouse calyx of Held synapses in acute brainstem slices in the presence of 1.7 mM Ca^{2+} and 1.3 mM Mg^{2+} in the bath solution. V_h was −80 mV and −70 mV for pre- and postsynaptic recordings, respectively. eEPSCs were recorded in the presence of 1 mM kynurenic acid (kyn) in the bath to minimize postsynaptic AMPAR saturation and desensitization. N = number of mice, n = number of synapses, n.s. = not statistically significant.